Meteorol Atmos Phys 84, 1–10 (2003)
DOI 10.1007/s00703-002-0574-6

Meteorology and Atmospheric Physics
Printed in Austria

School of Meterology, University of Oklahoma, Norman, OK, USA

The performance of an $E - l$ scheme for the atmospheric boundary layer in a mesoscale model with grid spacing as small as 1 km

B. H. Fiedler and **F. Kong**

With 9 Figures

Received June 7, 2002; accepted August 13, 2002
Published online: February 20, 2003

Summary

A new $E - l$ boundary layer scheme is tested within the U.S. Navy's COAMPS model. The goal is to give COAMPS the capability to simulate mesoscale cellular convection. The new scheme is aimed to be consistent with both classic results for clear entrainment and recent calibrations, derived from large-eddy simulations, for entrainment into smoke clouds and water clouds. A parameter is included in the scheme that allows sub-grid transport to be reduced so that, when the model has 2 km grid spacing or less, more of the transport is forced to occur in resolved convection. At 2 km grid spacing, the scheme allows COAMPS to simulate the break up of a stratocumulus cloud deck into mesoscale cellular convection.

1. Introduction

Mesoscale cellular convection is a pattern of clouds that often occurs in a stratocumulus-capped boundary layer. The individual convection cells are larger than the cumulus scale, and contain many cumulus elements. Mesoscale cellular convection has been reviewed – and perhaps better named as mesoscale shallow convection – by Atkinson and Zhang (1996). Operational weather forecast models are always being given ambitions for finer resolution. Even before these models reach a resolution where cumulus can be resolved, the models will confront the ability to skillfully represent mesoscale cellular convection and its ensuing impact on radiation and drizzle. This article aims to contribute towards that skill.

A recent numerical simulation of mesoscale cellular convection is Müller and Brümmer (1999). That exercise is typical in that the mesoscale cellular convection is modeled at high resolution in a small domain, rather than in an operational forecast model. In Müller and Brümmer (1999), the domain size is square with width 12.8 km and a horizontal grid spacing of 200 m. Other such examples are Shao and Randall (1996), who used a two-dimensional domain with width 32 km and a grid spacing of 250 m, and Fiedler and Khairoutdinov (1994), for which the model was dimensionless but effectively 16 km square with 125 m grid spacing. Here we offer a simulation of mesoscale cellular convection in a domain 350 km by 700 km with a horizontal grid spacing of 2 km. The model for this demonstration is COAMPS, the non-hydrostatic operational model of the United States Navy (Hodur, 1997).

The current operational boundary layer scheme of COAMPS is not used in any of the investigations or demonstrations in this article. Rather, the scheme of Fiedler (2002) has been

implemented into COAMPS. The $E-l$ scheme of Fiedler (2002) was studied within a one-dimensional model. The scheme uses the non-local mixing length formulation of Bougeault and Lacarrère (1989), but is otherwise very simple. The scheme has two adjustable parameters (multipliers) that control how the mixing length is used in the calculation of the diffusivity and the dissipation rate. The parameters are tuned to produce the proper performance of a clear, convective boundary layer: proper magnitudes of turbulence kinetic energy within the boundary layer, and proper rates of entrainment. In Fiedler (2002), this tuning causes the scheme to entrain too much into smoke clouds and water clouds.

The idealized tests of Fiedler (2002) – clear, smoky and cloudy – are then conducted with this revised COAMPS model. With 72 km grid spacing, which renders the simulation essentially one-dimensional, the performance with smoke clouds has fortuitously improved a bit, but the performance with clear conditions and cloudy conditions is otherwise very close to Fiedler (2002).

The implementation into COAMPS allows for the idealized tests to be conducted with a horizontal grid spacing that allows for resolved convection. However, the clear and smoke tests at 1 km grid spacing do not grow resolved convection from small perturbations, and the performance is identical with a one-dimensional test. In the cloud test, convective fluctuations develop, but only after about six hours into the integration. However, the entrainment rate increases and the average liquid water path is decreased, thus deviating even further from the calibration offered by Moeng (2000).

The lack of resolved convection in the clear and smoky tests with 1 km grid spacing raises the question about whether the $E-l$ scheme is doing its job too well. The multiplier for the eddy diffusivity is, evidently, large enough to give sufficiently vigorous transport that both diminishes the unstable lapse rate and stabilizes any incipient convective fluctuations. When the multiplier for the diffusivity is reduced to 30% of the standard value, the performance at 72 km grid spacing suffers from too little entrainment, as expected. However, at 1 km grid spacing, the proper performance is restored for all three tests, with resolved convection now contributing to the entrainment. The average liquid water path is also increased, becoming closer to the calibration offered in Moeng (2000). The cloud test, at either 1 km or 2 km grid spacing, shows clouds with a cellular structure in which the cells broaden with time, as in mesoscale cellular convection.

In a final demonstration, COAMPS is applied to a cold air outbreak over the Yellow Sea, at 2 km grid spacing. With the standard scheme, meaning without the reduction of the diffusivities, an unbroken stratus cloud deck exists for the first 350 km, where the satellite image shows convection. With the reduction, the stratus cloud immediately breaks into a more spectacular array of mesoscale cellular convection, consistent with what is observed from satellite imagery.

2. The non-local mixing length

The new boundary layer scheme that we implemented into COAMPS is identical to the one described in Fiedler (2002). The turbulent length scale $\lambda(z)$ is predicted with the non-local integrals as in Bougeault and Lacarrère (1989). At a given elevation z, λ is calculated as the geometric mean of two length scales: the distances a parcel could travel adiabatically upward or downward against the work of buoyancy if all its turbulent kinetic energy were converted to gravitational potential energy. Numerical evaluation of these integrals in a finite-difference model requires some care. In very stable regions, the length scale may become less than the grid interval. In those regions, a casual use of the trapezoidal rule will lead to a large discrepancy with the continuous equations. Details of how to accurately evaluate these integrals appears in Appendix A.

The non-local mixing length formulation was originally proposed by Bougeault and André (1986) in their third-order turbulence-closure model in an effort to overcome unstable numerical oscillations due to radiative cooling near cloud top. Bougeault and Lacarrère (1989) adapted the non-local mixing length into a two-dimensional version of a mesobeta-scale model to study orography-induced turbulence flows. Cuxart et al (2000) further developed the scheme for use in the Météo-France Meso-NH model, with motivations similar to our own. As in our investigation, they were concerned with developing a scheme that works in both one-dimensional

simulations and in three-dimensional simulations. However, the three-dimensional simulations they were concerned with had horizontal grid spacing from 50 m to 160 m, or were so-called large-eddy simulations. We are not concerned with grid spacing less than 1 km.

We do not know whether the use of the nonlocal mixing length is essential to the success that was achieved here. We found the concept appealing, as well as productive. The lack of abrupt changes in length scale at grid intervals that have become stable, or marginally saturated, is certainly more consistent with the notions of how large eddies would function in nature.

The dissipation rate of turbulent kinetic energy E is assumed to be

$$\frac{\alpha_E}{\lambda}E^{3/2}. \tag{1}$$

The diffusivity for all quantities is assumed to be

$$K = \beta\alpha_K\lambda\sqrt{2E}. \tag{2}$$

The factor β is new here. In Fiedler (2002), $\beta=1$, and the constants $\alpha_E=0.5$ and $\alpha_K=0.25$ were chosen to give proper results for a clear, convective boundary layer. These values for α_E and α_K are retained here. Such tuning also provides adequate performance for smoky and cloudy boundary layers, as will be reviewed in the next section. For reasons stated in the Introduction, we will also experiment with $\beta=0.3$, which in cloud-topped boundary layers at high resolution will be shown to have a beneficial effect.

3. Performance at 1 km, 2 km and 72 km grid spacing

The clear, smoke and cloud tests are described in Fiedler (2002). Success in the clear and smoke tests is assessed rather simply, by inspecting buoyancy flux profiles. Such profiles with horizontal grid spacing of 72 km and $\beta=1$ are shown in Fig. 1. In the clear test, the downward flux of buoyancy, resulting from entrainment, is 0.25 times the surface flux. This ratio is within the realm of uncertainity of the oft quoted value of 0.2. In the smoke test, the value of the positive flux, extrapolated to the inversion from the linear region near the lower boundary, would be about equal in magnitude to the maximum downward (negative) flux. This indicates that 50% of the radiative cooling is being compensated for by entrainment. For reasons unknown, the performance is better than in Fiedler (2002), which had about 75% of the radiative cooling being compensated for by entrainment. The performance here is more in accord with the performance of high-resolution, three-dimensional codes cited in Bretherton et al (1999), which also had about 50% compensation.

Further experiments with the clear and smoke tests will be assessed by comparing the potential

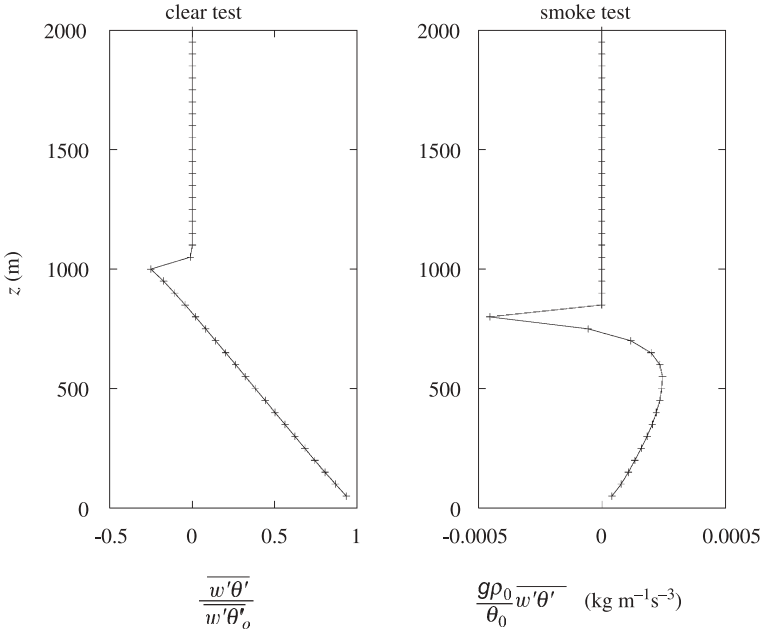

Fig. 1. Buoyancy fluxes in the clear and smoke test, averaged over the last 15 minutes of a 12 hour integration

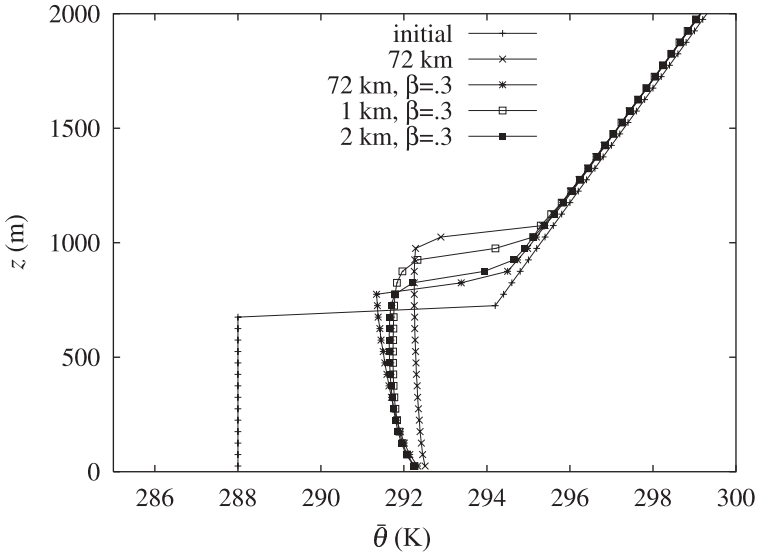

Fig. 2. Clear test with the revised COAMPS. Profile of potential temperature at the initial time and at 12 hours. $\beta = 1$, unless otherwise noted

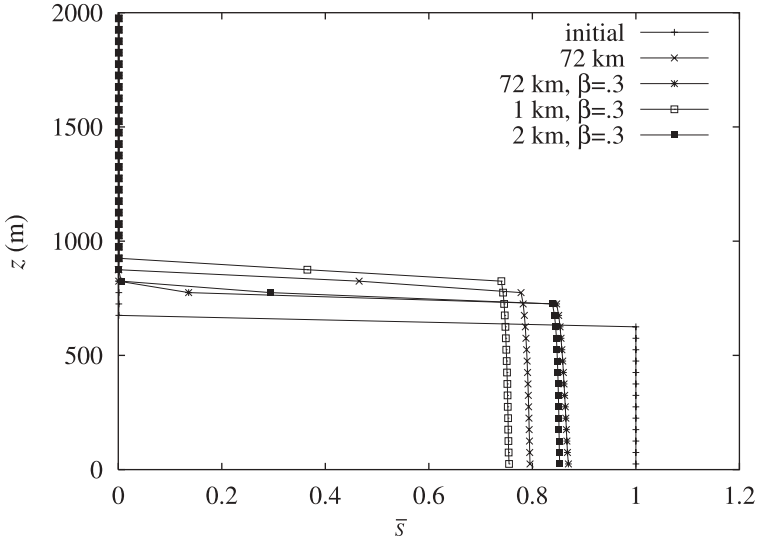

Fig. 3. Smoke test with the revised COAMPS. Profile of smoke concentration at the initial time and at 12 hours. $\beta = 1$, unless otherwise noted

temperature and smoke profiles at 12 hours. With the performance with $\beta = 1$ and 72 km grid spacing having been established as desirable, an assessment of the deviation from desired performance can be made by comparing the boundary layer depth evident in the profiles. These profiles are seen in Figs. 2 and 3. For the clear test, with $\beta = .3$, the entrainment rate is reduced to less than 50% of the value with $\beta = 1$, unless the grid spacing is decreased to 1 km. For the grid spacing of 1 km, entrainment by resolved convection is able to restore the entrainment rate to nearly the desired value. The same judgment is made about the smoke tests seen in Fig. 3. With $\beta = 1$, the clear and smoke simulations with a grid spacing of 1 km or 2 km produce the same results as 72 km grid spacing, and therefore are not plotted. If resolved convection is not desired in the forecast, but rather the desire is for fidelity with the 72 km result for the clear and smoke simulations, then $\beta = 1$ would certainly be preferred over $\beta = 0.3$. The point here is that using $\beta = 0.3$ and a grid spacing of 1 km does little, if any, harm to the behavior of the horizontal average in the clear and smoke tests. In the simulations with clouds, there will be an obvious benefit to resolving convection.

The assessment of the cloud test, at various grid spacings, with or without a reduced value of β, is shown in Fig. 4. The radiation scheme is not the idealized one used in Moeng (2000), and Fiedler (2002), but is the operational

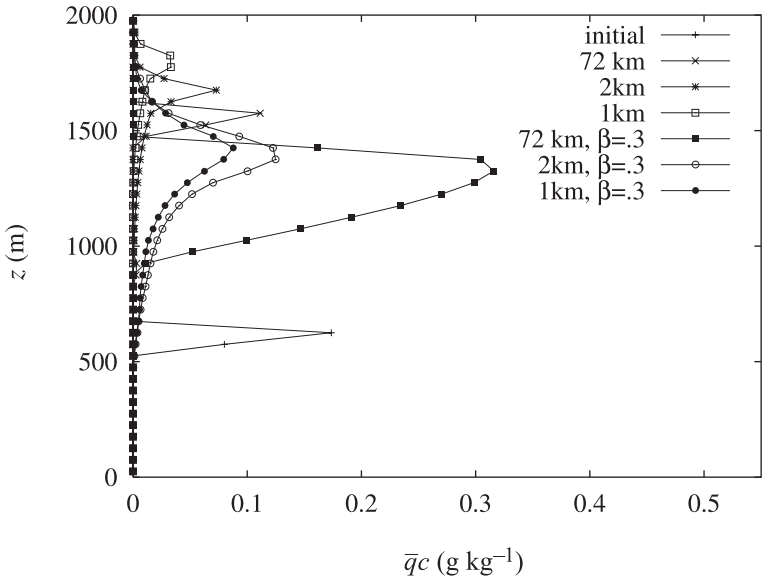

Fig. 4. Cloud test with the revised COAMPS. Profile of liquid water concentration at the initial time and at 12 hours. $\beta = 1$, unless otherwise noted

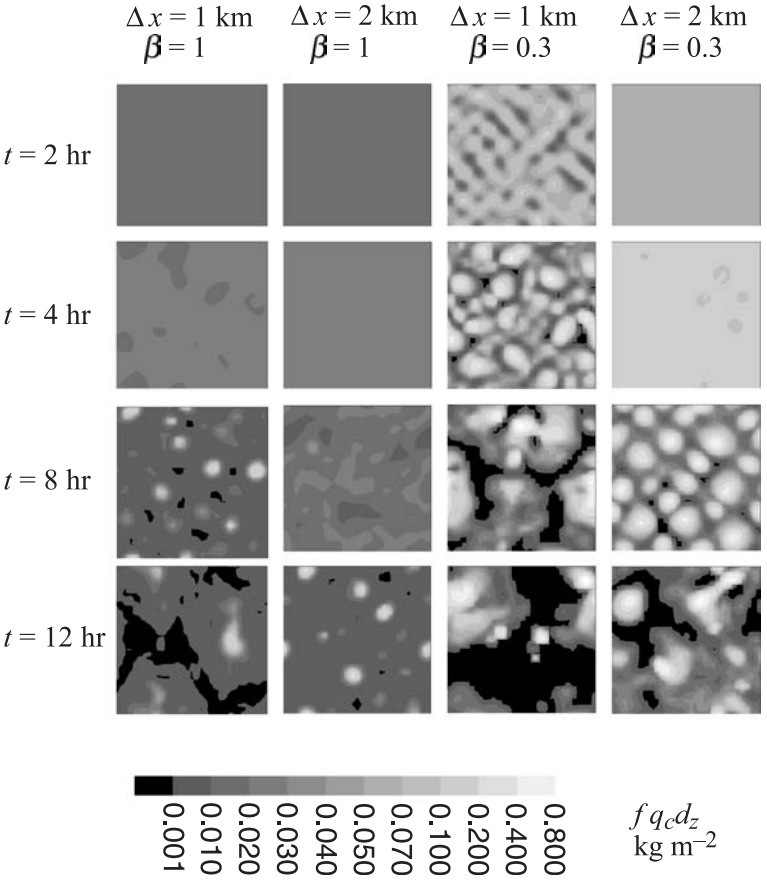

Fig. 5. Liquid water path across the horizontal domain, for some of the cloud tests. Domain width is 32 km for $\Delta x = 1$ km and, 64 km for $\Delta x = 2$ km

COAMPS scheme, though with the cosine of the zenith angle fixed at 0.3 for the entire integration. The cloud-top radiation in the COAMPS simulation is about 85 W m^{-2}, in Fiedler (2002) the maximum value is 74 W m^{-2}. The COAMPS simulation has some minor solar absorption and cloud-base warming; the idealized scheme in Fiedler (2002) has none.

For 72 km and $\beta = 1$, the result is similar to Fiedler (2002), producing about $w_e = 0.020$ m s^{-1} over the last six hours. The average liquid water path over the last 15 minutes is 8.5 g m^{-2}, in

Fiedler (2002) it was 14.4 g m^{-2}. The cloud is too thin by the standards of the parameterization of Moeng (2000), which predicts $w_e = 0.008$ m s^{-1} for a liquid water path of 8.5 g m^{-2}. Figure 4 shows that, with $\beta = 1$, the simulations with a grid spacing of 1 km and 2 km produce still deeper entrainment with thinner clouds; resolved convection is now contributing to the entrainment. Figure 5 shows a plot of liquid water path across the domain, at various times. For $\beta = 1$, the cloud is becoming patchy after 8 hr, as would be expected for a thin cloud layer.

Figure 5 also shows the simulations with $\beta = 0.3$. With 1 km grid spacing, the breakup looks much more natural, beginning early in the simulation with the cell size gradually increasing. The simulation with 2 km grid spacing also produces a natural-looking cell structure, though it is a bit sluggish in starting. All the simulations with 2 km grid spacing or less were initialized with random fluctuations in the temperature field of amplitude less than 0.1 K.

Returning to Fig. 4, we see that, with $\beta = .3$, the entrainment is a bit less and the liquid water path substantially greater. However, even the very thick cloud for 72 km grid spacing and $\beta = .3$, which has a liquid water path of 100 g m^{-2}, does not allow the formula of Moeng (2000) to predict the simulated entrainment rate of $w_e = 0.16$ m s^{-1}. The formula predicts $w_e = .012$ m s^{-1}. A liquid water path of 300 g m^{-2} is needed in that formula to predict $w_e = .016$ m s^{-1}. Nevertheless, using $\beta = .3$ and grid spacing less than or equal to 2 km, moves the results toward those of Moeng (2000), and allows for realistic-looking boundary layer convection. That having been said, it is possible that the formula of Moeng (2000) is not providing the best entrainment standard.

4. Application to mesoscale cellular convection

Here we use COAMPS, with the new scheme, to simulate a cold-air outbreak over the Yellow Sea that occurred on January 25, 2000. During the outbreak, the cold northerly flow blowing across the warm Yellow Sea produced a broad area of mesoscale cellular convection (MCC), as seen in Fig. 6.

Although COAMPS has a capability for multiple nested grids, this simulation has a single grid. The grid spacing in the horizontal is 2 km and

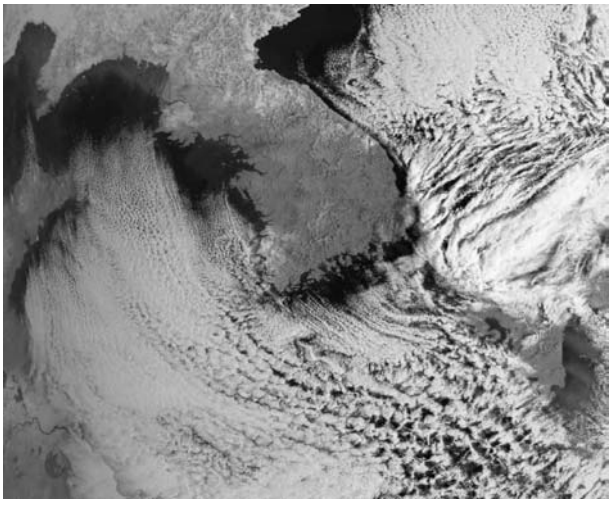

Fig. 6. NOAA-15 AVHRR image over the Yellow Sea at 23:36:09 UTC, January 25, 2000

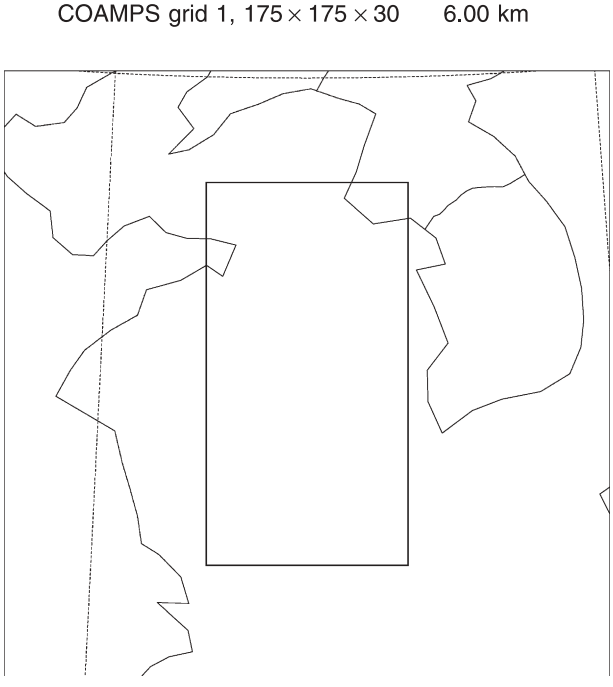

Fig. 7. The black rectangle shows a 350 km × 700 km region that will be simulated with COAMPS

there are 45 vertical levels. The cloud is always below 1900 m, where the vertical grid interval is always less than 100 m. The results for the clear and smoke tests indicated that a grid spacing of 2 km would not be small enough to resolve convection, and the cloud test showed that a 2 km spacing was not as capable as a 1 km spacing. Nevertheless, we are able to make an effective demonstration here with a 2 km grid spacing.

The rectangle in Fig. 7 shows the location of the COAMPS domain. The domain has

175×350 grid points in the horizontal, centered at 35.3° N and 124.0° E, covering a 350 km by 700 km region over the Yellow Sea. The model initial conditions use first-guess fields from the Navy Operational Global Atmospheric Prediction System (NOGAPS) data, modified by automated data processing observations through a multivariate optimum interpolation analysis procedure. The NOGAPS data also provides the lateral boundary conditions throughout the 24 h simulation process. The large time step used for integrating the advective mode is 10 s and the time-splitting ratio for the acoustic mode is 2.

Figure 8 shows simulations for $\beta = 1.0$ and $\beta = 0.3$. Unlike the satellite imagery in Fig. 6, the simulation with $\beta = 1.0$ produces a solid stratiform cloud deck in the northern half of the computational domain. With $\beta = 0.3$, the MCC

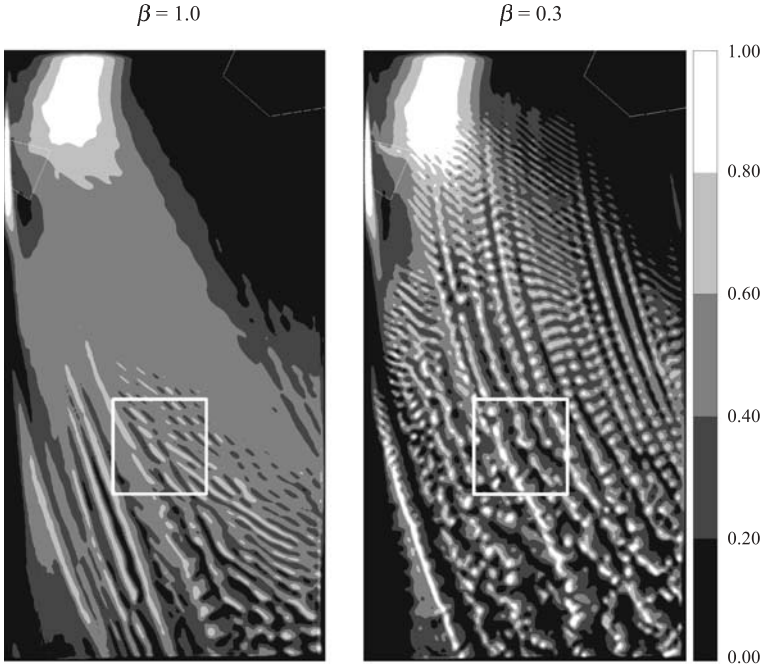

Fig. 8. COAMPS simulation over the Yellow Sea, showing liquid water path in kg m^{-2}. Left is $\beta = 1$. Right is $\beta = 0.3$. $\Delta x = \Delta y = 2$ km. 24 hour forecast valid at 00:00 UTC January 26, 2000. The square in the center of the domain is the region for which horizontal averages are computed for the profiles in Fig. 9

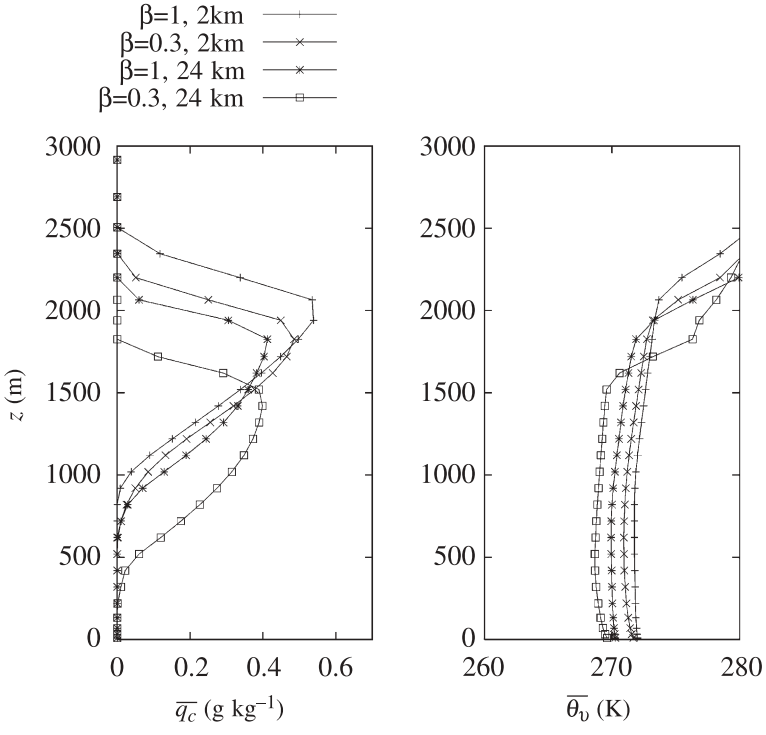

Fig. 9. Vertical profiles of q_c and θ_v for the simulations with 2 km grid spacing shown in Fig. 8, averaged over the square region denoted in Fig. 8. Also shown are profiles for 24 km grid spacing

structure developed in the northern half of the domain after 3 hours. The MCC structure is not entirely skillful. For example, the satellite imagery shows cloud streets on the upwind edge of the cloud field, but the simulation shows a cross-wind pattern.

Figure 9 shows the profiles of q_c and θ_v, averaged over a 80 km × 80 km square in the center of the cloud field indicated in Fig. 8. Despite the differences in the value of β, both simulations with 2 km grid spacing show similar profiles. The similarity results from resolved convection compensating for reduced subgrid transport when $\beta = 0.3$.

Figure 9 also shows profiles for simulations with a grid spacing of 24 km (for which the liquid water path is not plotted). Comparing those profiles, the simulation with $\beta = 0.3$ has significantly less entrainment than the simulation with $\beta = 1.0$. Note also that both simulations with 24 km grid spacing have less cloud water than those with 2 km grid spacing. We attribute this to the fact that the total water in the boundary layer is reduced by about 10% with the use of 24 km grid spacing, perhaps due to a different representation of the coastline. Nevertheless, the comparison of these four simulations supports a claim that using 2 km grid spacing with $\beta = 0.3$ does allow for resolved convection to accurately replace the entrainment of subgrid convection.

In Fig. 4, we saw a ten-fold increase in liquid water path with the use of $\beta = 0.3$ and a grid spacing of 72 km. Here, Fig. 9 shows no significant increase in liquid water path with the use of $\beta = 0.3$. The Bowen ratio in this simulation is near 1.0, in the region of the averaging square. In Fig. 4 it was 0.04. So this different behavior is not necessarily contradictory.

5. Conclusions

A simple $E - l$ scheme for a boundary layer has been optimized (meaning "tuned") to allow COAMPS to produce MCC. The optimization consists of two steps. First, the scheme is tuned to entrain properly when used in a one-dimensional, or column, simulation. Secondly, the diffusivity is parameterized to be reduced when the model is run with 1 km or 2 km grid spacing, with the intent of having the resolved scale convection perform the role of sub-grid diffusion. Here we were successful with simply imposing a reduction of diffusivities to 30% of the value that was optimal in one-dimensional simulations. There was no reason to anticipate that such a simple modification would allow for proper rates of entrainment in the presence of resolved convection in all the tests, but that was the providential, empirical result with our particular boundary layer scheme.

The ability of a boundary layer scheme both to resolve convection and also to entrain properly is a desirable feature for a model. When the scheme is used in COAMPS with 2 km grid spacing, COAMPS is able to give a credible simulation of mesoscale cellular convection.

Appendix A

The mixing length

At a given elevation z, λ is calculated as the geometric mean of two length scales: the distances a parcel could travel adiabatically upward and downward against the work of buoyancy if all its turbulent kinetic energy were converted to gravitational potential energy. For an air parcel with mean turbulence kinetic energy $E(z)$, the maximum upward displacement (λ_{up}) and downward displacement (λ_{down}) can be calculated by satisfying the following integrals:

$$E(z) = \int_z^{z+\lambda_{\text{up}}(z)} \frac{g}{\overline{\theta_v}(z')} [\overline{\theta_v}(z') - \overline{\theta_v^*}(z, z')] dz' \tag{A.1}$$

and

$$E(z) = \int_z^{z-\lambda_{\text{down}}(z)} \frac{g}{\overline{\theta_v}(z')} [\overline{\theta_v}(z') - \overline{\theta_v^*}(z, z')] dz', \tag{A.2}$$

where $\overline{\theta_v^*}(z, z')$ is calculated assuming an adiabatic transformation from the pressure at z to the pressure at z'. Let

$$f(z, z') \equiv \overline{\theta_v}(z') - \overline{\theta_v^*}(z, z'). \tag{A.3}$$

With $\overline{\theta_v}(z')$ in the denominator in (A.1) approximately equal to $\overline{\theta_v}(z)$, the integral (A.1) can be written as

$$E(z) = \frac{g}{\overline{\theta_v}(z)} \int_z^{z+\lambda_{\text{up}}(z)} f(z, z') dz'. \tag{A.4}$$

Note that $f(z, z) = 0$. Consider the special case of a deep layer of linear stratification:

$$f(z, z') = (z' - z) \frac{\partial f}{\partial z'}. \tag{A.5}$$

Equation (A.4) is

$$E(z) = \frac{g}{\overline{\theta_v}(z)} \frac{\partial f}{\partial z'} \frac{\lambda_{\text{up}}^2}{2}. \tag{A.6}$$

We need to keep (A.6) in mind when we develop a discrete approximation to (A.4). With

$$s(z) \equiv E(z)\frac{\overline{\theta_v}(z)}{g}, \tag{A.7}$$

(A.4) can be written as

$$s(z) = \int_z^{z+\lambda_{\rm up}(z)} f(z,z')dz'. \tag{A.8}$$

(a) The mixing length in a discrete model

We seek $\lambda_{\rm up}$ at discrete values z_n. To find a value of $\lambda_{\rm up}(z_n)$ we first seek the largest value of $N \geq n$ that allows

$$S_n = \sum_{k=n}^{k=N} \frac{1}{2}[f(z_n,z_k)+f(z_n,z_{k+1})](z_{k+1}-z_k) \leq s(z_n). \tag{A.9}$$

In the above we have used the trapezoidal approximation for an integral. We then seek

$$s(z_n) - S_n = \int_{z'=z_{N+1}}^{z'=z_n+\lambda_{\rm up}} f(z_n,z_{N+1}) + \frac{f(z_n,z_{N+2})-f(z_n,z_{N+1})}{z_{N+2}-z_{N+1}}(z'-z_{N+1})dz' \tag{A.10}$$

or solve for δ in

$$s(z_n) - S_n = f(z,z_{N+1})\delta + \frac{f(z_n,z_{N+2})-f(z_n,z_{N+1})}{z_{N+2}-z_{N+1}}\frac{\delta^2}{2}, \tag{A.11}$$

where $\delta \equiv z_n + \lambda_{\rm up} - z_{N+1}$. Therefore, having found z_{N+1} and δ,

$$\lambda_{\rm up}(z_n) = z_{N+1} - z_n + \delta. \tag{A.12}$$

If (A.9) is not satisfied for any $N \geq n$, then $S_n = 0$, and, in (A.11), $N+1 = n$.

Consider strong stratification: suppose $S_n = 0$ and $z_{N+1} = z_n$. Equation (A.11) is then

$$s(z_n) = \frac{f(z_n,z_{n+1})-f(z_n,z_n)}{z_{n+1}-z_n}\frac{\delta^2}{2} \tag{A.13}$$

which is the same as (A.6).

A similar computation is made for $\lambda_{\rm down}$. Finally,

$$\lambda(z_n) = [\lambda_{\rm down}(z_n)\lambda_{\rm up}(z_n)]^{1/2}. \tag{A.14}$$

(b) The LCL

The calculation of $\theta_v^*(z,z')$ in (A.1) and (A.2) may require a saturation adjustment, adding to the expense of evaluating the integrals. In order to save computing time, the scheme should recognize when it is unnecessary to attempt a saturation adjustment. In calculating $\lambda_{\rm down}$ in (A.2), the test parcel of air, for which $\theta_v^*(z,z')$ is being calculated, will not require an attempt at saturation adjustment once q_c has disappeared, because saturation mixing ratio monotonically increases with pressure. After $q_c = 0$, θ_v^* will be unchanging.

In calculating (A.1), a lifting condensation level (LCL) should be calculated. Below that level, no attempt at saturation adjustment should be made, and θ_v* will be unchanging. In order to save computing time, a lookup table is used to determine the air pressure at which saturation would occur.

For saturation vapor pressure e_s, COAMPS uses

$$e_s(T) = 611.\ e^{f(T)}\text{Pa}, \tag{A.15}$$

where

$$f(T) \equiv \ln(10)\ 7.5\ \frac{T-273.16}{T-35.86} \tag{A.16}$$

and T is temperature in degrees K. Up to the point of saturation, q_v will be conserved and vapor pressure will be

$$e = \frac{q_v p}{.622}. \tag{A.17}$$

In an unsaturated adiabatic expansion,

$$p \equiv p_o\left(\frac{T}{\theta}\right)^{c_p/R}, \tag{A.18}$$

and using this in (A.17), we have $e(T)$ for the expanding parcel. A lifting condensation temperature is found by solving $e(T) = e_s(T)$, for T. The temperature can be converted to a lifting condensation pressure using (A.18). The equation $e(T) = e_s(T)$ can be written:

$$\frac{q_v p_o}{0.622}\left(\frac{\theta_o}{\theta}\right)^{c_p/R}\left(\frac{T}{\theta_o}\right)^{c_p/R} = 611e^{f(T)} \tag{A.19}$$

or

$$\ln\left[\frac{1}{611}\frac{q_v p_o}{0.622}\left(\frac{\theta_o}{\theta}\right)^{c_p/R}\right] + \frac{c_p}{R}\ln\left(\frac{T}{\theta_o}\right) = f(T), \tag{A.20}$$

where we choose to use $p_o = 10^5$ Pa and $\theta_o = 300$ K. Let

$$Y \equiv 10\ln\left[\frac{1}{611}\frac{q_v p_o}{0.622}\left(\frac{\theta_o}{\theta}\right)^{c_p/R}\right] \tag{A.21}$$

and

$$X(T,Y) \equiv \frac{Y}{10\ln(10)7.5} + \frac{1}{\ln(10)\ 7.5}\frac{c_p}{R}\ln\left(\frac{T}{\theta_o}\right). \tag{A.22}$$

Equation (A.20) can be written as

$$X(T,Y) = \frac{T-273.16}{T-35.86}. \tag{A.23}$$

A solution for T can be found by iterative improvement of

$$T = \frac{273.16 - 35.86X(T,Y)}{1-X(T,Y)}. \tag{A.24}$$

Values of Y from -466 to 51 used in (A.24) give $T(Y)$ spanning from 96 K to 404 K. A lookup table is made for integer values of Y.

Acknowledgments

This research was supported by the Department of Defense of the U.S.A. under grant N00014-96-1-1112. Dr. Vince Wong contributed to the coding of the new scheme.

References

Atkinson BW, Zhang JW (1996) Mesoscale shallow convection in the atmosphere. Rev Geophys 34: 403–431

Bougeault P, André JC (1986) On the stability of the third-order turbulence closure for the modeling of the stratocumulus-topped boundary layer. J Atmos Sci 43: 1574–1581

Bougeault P, Lacarrère P (1989) Parameterization of orography-induced turbulence in a mesobeta-scale model. Mon Wea Rev 117: 1872–1890

Bretherton CS, MacVean MK, Bechtold P, Chlond A, Cotton WR, Cuxart J, Cuijpers H, Khairoutdinov M, Kosovic B, Lewellen D, Moeng CH, Siebesma P, Stevens B, Stevens DE, Sykes I, Wyant MC (1999) An intercomparison of radiatively driven entrainment and turbulence in a smoke cloud, as simulated by different numerical models. Q J R Meteorol Soc 125: 391–423

Cuxart J, Bougeault P, Redelsperger JL (2000) A turbulence scheme allowing for mesoscale and large-eddy simulations. Quart J Roy Meteorol Soc 126: 1–30

Fiedler BH (2002) Grid adaption and its effect on entrainment in an $E-l$ model of the atmospheric boundary layer. Mon Wea Rev 130: 730–740

Fiedler BH, Khairoutdinov M (1994) Cell broadening in three-dimensional thermal convection between poorly conducting boundaries: Large eddy simulations. Beitr Phys Atmos 67: 235–241

Hodur RM (1997) The Naval Research Laboratory's coupled ocean/atmosphere mesoscale prediction system (COAMPS). Mon Wea Rev 125: 1414–1430

Moeng CH (2000) Entrainment rate, cloud fraction, and liquid water path and PBL stratocumulus clouds. J Atmos Sci 57: 3627–3643

Müller G, Brümmer B (1999) Roll convection within an arctic cold-air outbreak: interpretation of in situ aircraft measurements and spaceborne SAR imagery by a three-dimensional atmospheric model. Mon Wea Rev 127: 363–380

Shao Q, Randall DA (1996) Closed mesoscale cellular convection driven by cloud-top radiative cooling. J Atmos Sci 53: 2144–2165

Corresponding author's address: Dr. Brian Fiedler, School of Meteorology, EC 1310, 100 E. Boyd St., Norman, OK 73019, USA (E-mail: bfiedler@ou.edu)